Hindawi Publishing Corporation
Journal of Spectroscopy
Volume 2016, Article ID 2490128, 13 pages
http://dx.doi.org/10.1155/2016/2490128

Review Article

Light Manipulation by Single Cells: The Case of Diatoms

Edoardo De Tommasi

Institute for Microelectronics and Microsystems, National Research Council, Via Castellino 111, 80131 Naples, Italy

Correspondence should be addressed to Edoardo De Tommasi; edetommasi@na.imm.cnr.it

Received 29 September 2016; Accepted 27 October 2016

Academic Editor: Pedro D. Vaz

Diatoms are ubiquitous monocellular microalgae, responsible for about 20–25% of the global oxygen produced by photosynthesis. Living in environments where sunlight is not so easily accessible, evolution shaped diatoms in order to exploit light with high efficiency. In particular, diatoms are provided with an external, micro- and nanopatterned silica shell, the frustule, surprisingly similar to artificial photonic crystals and able to manipulate light in many different ways. The present paper reviews the most relevant studies on optical and photonic properties of diatoms that have been performed throughout the last years making use of SEM characterizations, transmittance measurements at different wavelengths, holographic microscopy, Raman spectroscopy and imaging, photoluminescence spectroscopy, and the predictive support of different numerical simulation algorithms.

1. Introduction

From insects to flowers to birds, nature offers several examples of organisms able to manipulate light just in virtue of micro- and nanoscaled architectures, without contribution of any pigment [1–4]. Among these, diatoms play a fundamental role due to their massive contribution (estimated around 20–25%) to global photosynthetic oxygen production [5]. Diatoms are ubiquitous and monocellular microalgae which dominate phytoplankton through tens of thousands of species, differing in dimension and shape [6]. Nevertheless, all the species share a common feature: the protoplasm is enclosed in a micro- and nanopatterned silica box, the frustule, constituted by two valves interconnected by a lateral girdle. Dimensions of frustules (from some millimeters to some microns) and of pores (from several microns to some tens of nanometers) and their more or less periodic arrangement are species-specific. Single valves can be made by a superposition of several layers, each characterized by pores of different dimensions and different geometrical distribution [7].

Starting from the shape of the frustule, we can distinguish between *centric* diatoms, characterized by circular symmetry and whose large majority is planktonic, and *pennate* diatoms, with elongated, bilaterally symmetric frustules and mainly inhabiting shaded areas in benthic and epipelic communities. Examples of single valves for different species are reported in Figure 1.

In Figure 2(a) the scheme of a generic frustule is represented. One-half (the *hypotheca*), formed by a *hypovalve* and relative lateral band, is inserted into an analogue, bigger structure (the *epitheca*), thus forming, as a whole, a sort of Petri-dish box that encloses the protoplasm of the cell.

Several hypotheses about the evolutionary advantages represented by the frustule have been proposed over the years. Surely it gives protection to the cell versus animal grazing and other noxious agents; secondly, it ensures a noticeable protective function against mechanical stress, supporting the greatest possible force with minimal amount of material in virtue of ribs and pores dissipating most of it [8]. The fact that diatoms are photosynthetic organisms living in environments where sunlight is often not so easily accessible, in conjunction with the extraordinary resemblance of frustule ultrastructures with those of photonic crystals [9], has induced both biologists and experts in optical properties of materials to hypothesize that frustule could play a fundamental role also in light manipulation.

In the following we want to offer a wide overview of the photonic properties of frustules identified at present and, when possible, describe their relationship with the functionalities of the living cell; furthermore, the main spectroscopic

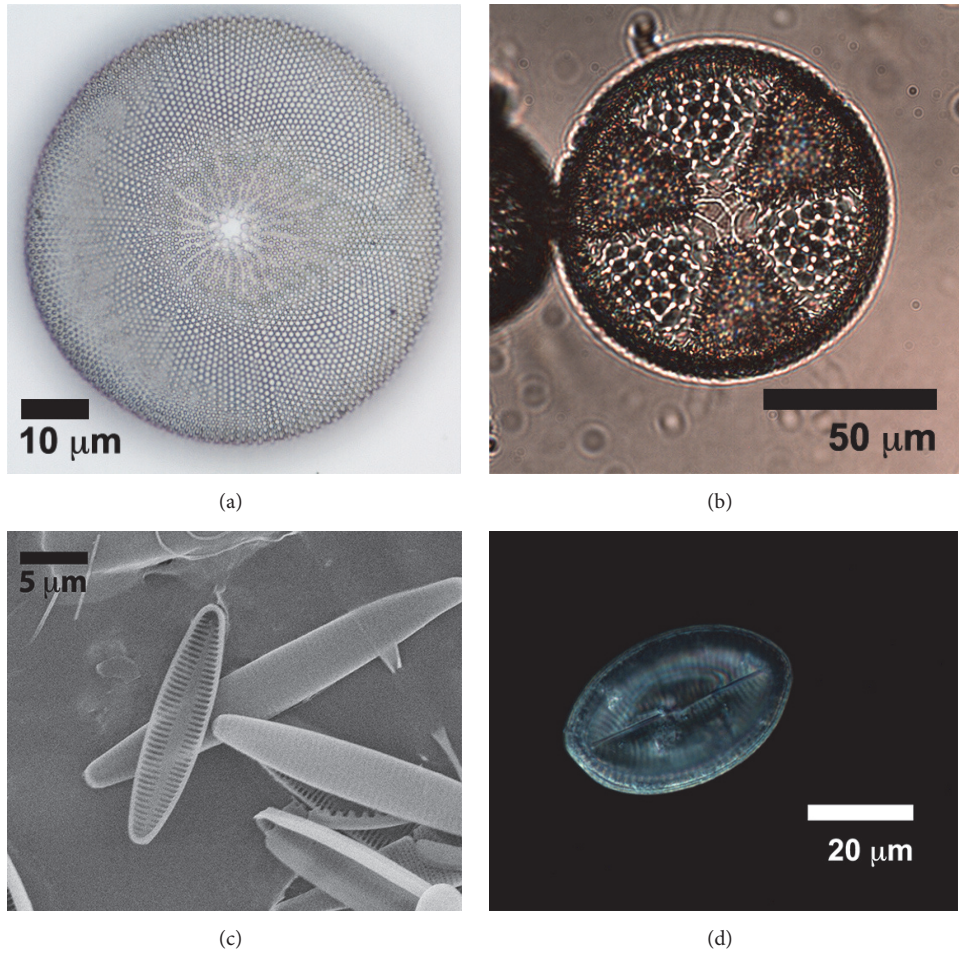

Figure 1: Single valves of *Coscinodiscus wailesii* (a) and *Actinoptychus senarius* (b) centric diatoms. Examples of pennate diatoms: arctic unspecified species (c) and *Cocconeis scutellum* (d) valves.

and imaging techniques aimed at the identification and characterization of these properties are examined; finally, most of their possible applications are illustrated.

2. Chemical Characterization of the Frustule

Before examining the optical properties of diatom frustules and how these properties influence the living cell, it can be useful to analyze their chemical composition. Usually, in Raman spectra of single diatom frustules acquired after removal of organic content, several peaks related to hydrated silica appear, as can easily be expected. Furthermore, peaks relative to organic impurities incorporated in the porous, siliceous matrix of the frustule (mainly C-H bonds) are also present [10]. In Figure 3 some Raman spectra acquired from a single valve of *Coscinodiscus wailesii* after removal of the organic content are reported. As stated above, mediating over 20 spectra acquired from different points of the valve we obtain typical bands relative to the hydrated siliceous matrix and trace organic compounds still present after protoplasm removal (mainly Si-O-Si and C-H stretching modes, respectively). Local signals associated with sulfur bonds are also detected (C-S and S-H bonds). This allows us to highlight another fundamental aspect of diatoms biology. It is known indeed [11] that diatoms and, in general, phytoplankton are deeply involved in sulfur global cycle. In a stage of their metabolism, they produce dimethyl sulfide (DMS), which is then emitted in the atmosphere, representing in fact the main natural source of atmospheric sulfur. Oxidized DMS is in turn involved in sulfur aerosols production, which contribute to cloud condensation and solar radiation scattering. Consequent variation in radiative balance of the Earth has influence on phytoplankton growth and relative sulfur production; in this way the sulfur cycle is properly self-regulated [12].

But sulfur compounds are also strictly involved in frustule formation. Since early Fifties, indeed, the role of sulfhydryl groups in silicates uptake by diatoms was experimentally observed [13]. In 1998 Hildebrand and coworkers [14] identified five silicon transporter genes in *Cylindrotheca fusiformis* whose corresponding amino acid sequences presented nine conserved cysteines; cysteines, together with methionines, are the only amino acids involved in protein synthesis which contain sulfur as part of their chemical structure. In 1999, the polypeptides involved in silica precipitation starting from silicic acid solutions, the so-called *silaffins*, were finally identified [15]. In general, the molecules involved in biosilica

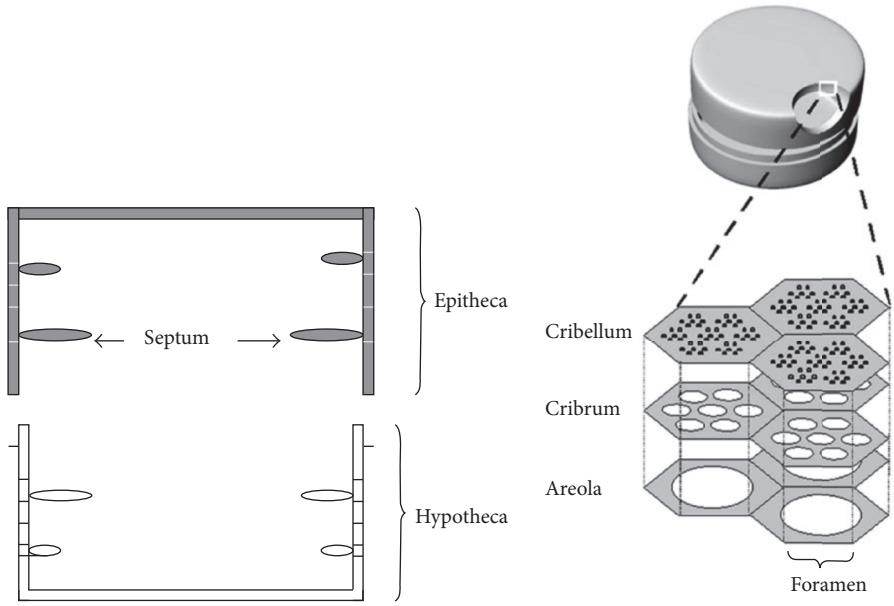

Figure 2: Schematic of a generic frustule (a) and of a centric diatom frustule (b) with cross-sectional profile of the valve. The inner layer with chambers called *areolae* is known as *foramen*. The roof of the areolae is called the *cribrum*, which contains a regular pattern of pores. The layer over the cribrum is a thin membrane known as *cribellum*, which is characterized by smaller pores. (b) is reproduced with permission from [7].

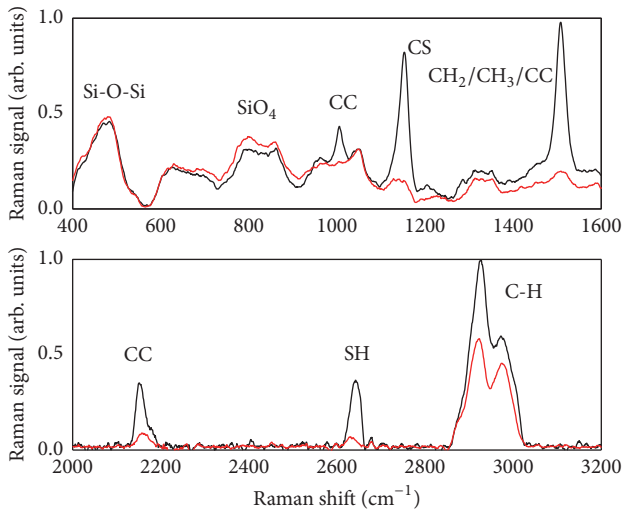

Figure 3: Raman spectra of a single valve of *C. wailesii* in the range 400–3200 cm^{-1} acquired after removal of organic content from the frustule. The red curves refer to the mean over 20 spectra acquired in different points of the valve. Black curves refer to the mean over three spectra where the presence of sulfur composites has been detected. The assignments of the bands are as follows: 450–550 cm^{-1}: Si-O-Si stretching vibrations; 800–850 cm^{-1}: SiO_4 symmetric stretching; 900–950 cm^{-1}: SiO_3/SiO_2 symmetric stretching (not indicated in figure for clarity purpose); 950–1050 cm^{-1}: CC aromatic ring chain vibrations; 1050–1100 cm^{-1}: SiO/SiO_2 symmetric stretching (not indicated in figure for clarity purpose); 1150–1200 cm^{-1}: CS; 1450–1550 cm^{-1}: $CH_2/CH_3/CC$; 2100–2250 cm^{-1}: CC; 2550–2600 cm^{-1}: SH; 2800–3000 cm^{-1}: C-H stretching vibration.

synthesis (silaffins, long-chain polyamines, frustulines, and cingulines [16]) and the corresponding genes are still far to be fully characterized in terms of functionalities and expression. All these lacking information will assume a fundamental role in the realization of frustules with desired morphology starting from single cells properly mutated.

3. The "Living Photonic Crystals"

A photonic crystal is defined as a spatial, periodic distribution of refractive index which, properly dimensioned, can inhibit propagation of light in specific wavelength ranges (the so-called *photonic bandgaps*). The whole mathematical formalism describing the optical behavior of a photonic crystal is the same which describes the electric properties of a semiconductor, where the periodic refractive index plays the role of the periodic electric potential, the photons are the analogous of the electrons, and the photonic bandgaps are the equivalent of the forbidden bandgaps separating valence and conductive bands [17].

A lot of insects, flora, and even birds possess, as part of their scales, cuticles, petals, and plumage, some submicrometric, periodic structures whose features have dimensions of the same order of magnitude of visible wavelengths and which act as photonic crystals [3, 4]. In the case of *Morpho rhetenor* butterfly, for example, blue radiation cannot propagate through the wings in virtue of ordered, periodic, nanometric ridges inside the wing scales which act as a sort of Bragg reflector [18]. Blue light is then scattered back, thus giving rise to what is called *structural* color, that

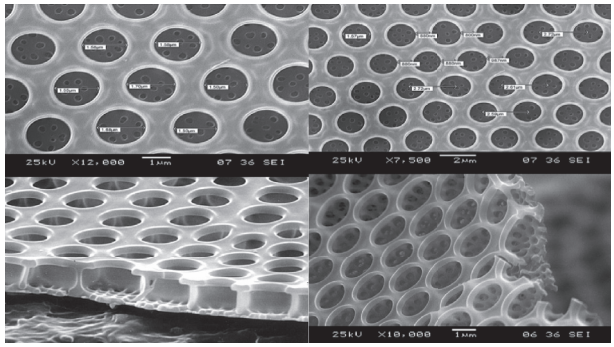

Figure 4: Details of a single valve of *C. wailesii*, reproduced with permission from [29].

is, a color that is not due to any pigment absorbing light at specific wavelengths but only to geometrical features of micro- and nanostructures and their refractive index contrast with respect to the surrounding environment.

Diatom frustules and valves present the most impressive resemblance with artificial photonic crystals [9], as it can be seen from Figure 4: a single layer of a single valve of *C. wailesii* can be described, in first approximation, by a photonic crystal slab with hexagonal lattice. Even though it has been numerically demonstrated that, for light propagating out of the plane defined by the slab, photonic bandgaps can be accessible even for refractive index contrasts as small as that of silica and air [19], they have not been experimentally observed yet; in any case, they can be hardly found for refractive index contrasts similar to that between silica and water/cytoplasm ($n \simeq 1.45$ and 1.34 in the visible range, resp.) and for light propagation in the plane defined by the slab [9, 20, 21].

In Figure 5(a) the result of numerical calculations based on Plane Wave Expansion (PWE) [22] and aimed at the reconstruction of the photonic band structure of a single layer of a single valve of *C. wailesii* diatom is shown: for light propagation in the plane of the valve no bandgap is present. Nonetheless, as we will see in last section, we are nowadays able not only to dope diatom frustules with molecules other than silica [23, 24], but also to obtain replicas of them choosing the proper material for a specific application [25–27]. In Figure 5(b), for example, the band structure for a valve made of titania (a material typically applied in optoelectronics) is reported, showing several photonic bandgaps for Transverse Electric (TE) polarization.

We have to keep in mind that, in a photonic crystal *slab*, the properties of a two-dimensional photonic band structure combine with that of a planar waveguide. Fuhrmann et al. [9], who for the first time introduced the analogy between diatom frustules and photonic crystals talking of diatoms as *"living photonic crystals,"* calculated the guided modes coupled into the girdle and valves of a *Coscinodiscus granii* frustule taking into account the influence of the associated photonic band structures. They also evaluated the penetration depth of the evanescent waves associated with the guided modes into the cell. It is known that, under dim lighting conditions, the chloroplasts (the organelles where photosynthesis takes place) tend to locate close to the frustule walls [28], thus well within the evanescent wave of the coupled modes. The evanescent field is expressed as

$$E(z) = E_0 \exp\left(-\frac{2\pi}{\lambda_0}\sqrt{n_{\text{eff}}^2 - n_m^2}\, z\right), \tag{1}$$

where n_{eff} is the effective refractive index of the frustule; n_m is the refractive index of the surrounding medium; λ_0 is the vacuum wavelength; and z is the direction perpendicular to the plane of the slab. It is thus straightforward that, for small refractive index contrasts (like the one between porous silica and water and/or cytoplasm), the evanescent wave can reach far into the living cell, letting an efficient optical coupling with the chloroplasts.

4. Light Collection and Confinement by a Single Diatom Valve

After considering the optical modes coupled to the girdle and valves, it is important to study the behavior of light impinging out of the plane of the valve, being transmitted by it and reaching the interior of the cell.

De Stefano et al. [29] firstly demonstrated the ability of a single valve of *C. wailesii*, about 150 μm in diameter, to confine red, coherent light in a tiny spot $< 10\,\mu$m at a distance of $\simeq$100 μm from the valve along the optical axis. The hypothesis was that this phenomenon, far to be ascribed to refraction by the valve disk, was due to the coherent superposition of the diffraction contributions coming from the single pores. The diffractive nature of the effect was confirmed by Noyes et al. [30]: making use of an Euler cradle (traditionally applied in X-ray diffraction characterization of crystal samples), they were able to analyze intensity and orientation of light transmitted by single valves of *C. wailesii* diatoms, after irradiation with blue (472 nm), green (543 nm), and red (633 nm) laser light. What they found is that red light is transmitted with more efficiency with respect to blue and green one, with a difference of 350% and 250%, respectively. Light which was not transmitted, reflected, or scattered by the valve was coupled into the guided modes already identified in [9] and described in the previous section. It has to be noticed that, in the interval between 630 and 675 nm of the optical spectrum, we can find the absorption maxima of chlorophylls *a* and *b*, the main molecules involved in photosynthesis [31]. Furthermore, the use of a broadband supercontinuum laser allowed retrieving diffraction patterns from a single valve of *C. wailesii* (so far the most studied diatom species in terms of photonic properties) [21]: the symmetry of the patterns is of course related to the symmetry of the pore spatial distribution of the valve (hexagonal for *C. wailesii*), while the spectral content of the diffracted light depends on the region of the valve which is illuminated.

Since diatoms interact with sunlight, the confinement of optical radiation transmitted by a single valve and its dependence by wavelength have been studied also starting from incoherent sources, for example, for *C. wailesii* [32–34], *C. centralis* [35], and *Arachnoidiscus* sp. valves [36].

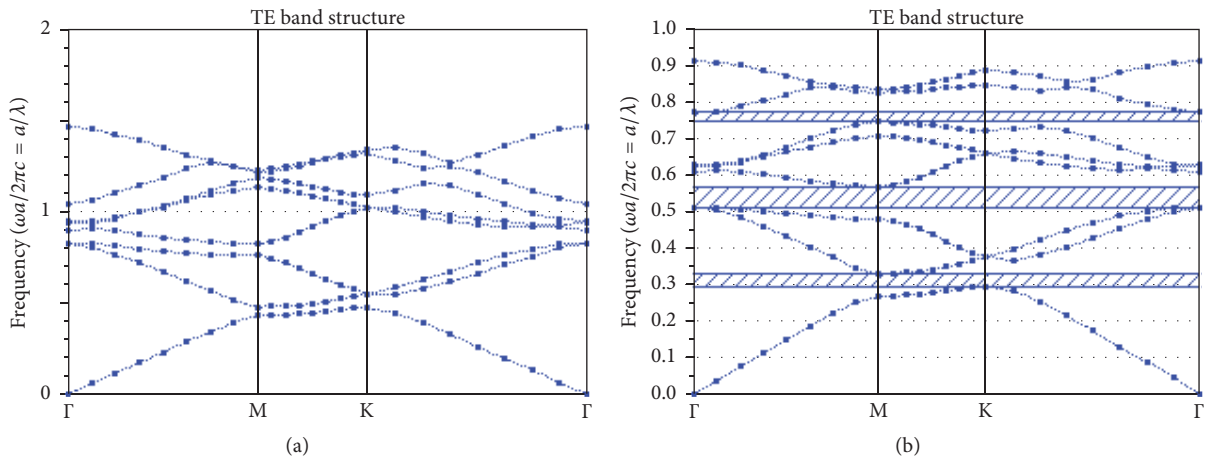

FIGURE 5: Calculated two-dimensional band structure of the inner layer of a single valve of *C. wailesii* diatom, with pores diameter $d = 1.4\,\mu$m and lattice constant $a = 1.8\,\mu$m (a). The same calculations have been performed substituting silica ($n = 1.45$) with titania ($n = 2.4$) (b). Calculations have been performed for Transverse Electric (TE) polarization.

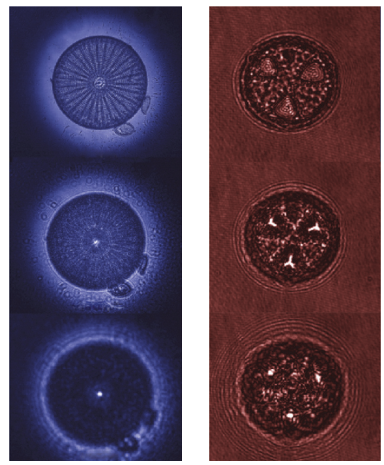

FIGURE 6: Light confinement induced by a single valve of *Arachnoidiscus* sp. (a) and *A. senarius* (b). See text for details.

In Figure 6(a), images of a single valve of *Arachnoidiscus* sp. diatom, illuminated by blue radiation ($\lambda = 460 \pm 5$ nm) coming from a halogen lamp properly filtered and collimated, are reported. Diatoms from *Arachnoidiscus* genus are characterized by a relatively big valve whose diameter is, on average, of about 200 μm; their mature frustule consists of several girdles, so that the overall length of it can overcome the diameter of the valve [37]. Images shown in figure have been acquired at different distances from the valve along the direction of propagation of light (z direction). It can be seen how, at specific distances ($z = 130\,\mu$m for the second row and $z = 670\,\mu$m for the third row) incident light is confined in a very bright hot spot, whose position along the optical axis strictly depends on the wavelength of the incoming radiation and on the medium in which the valve is suspended.

Both experimental data and numerical simulations based on Wide Angle Beam Propagation Method (WA-BPM) [32, 36] (see Figure 7 for *C. wailesii*) confirmed that these hotspots are the result of the coherent superposition of light diffracted from pores and edges of the valve (in case of *Arachnoidiscus* also the central flange and the radiating *costae* contribute to light diffraction). According to the dependence of diffraction angle from wavelength, the longer the wavelength is, the closer to the valve the hotspot takes place. This implies that, for sufficiently short wavelengths, the superposition of diffractive contributions takes place far beyond the frustule or it does not take place at all. This could be one of the mechanisms by which diatom frustules are able to protect the cell from harmful UV radiation, the other being absorption from the amorphous silica of the frustule itself. In case of *Arachnoidiscus*, for example, UVB transmitted radiation reaches the first, weak intensity peak at 500 μm from the valve (with values comparable to that of incident radiation), while for red light we have a first maximum at 90 μm from the valve and an intensity enhancement factor of more than 3 with respect to incident radiation [36].

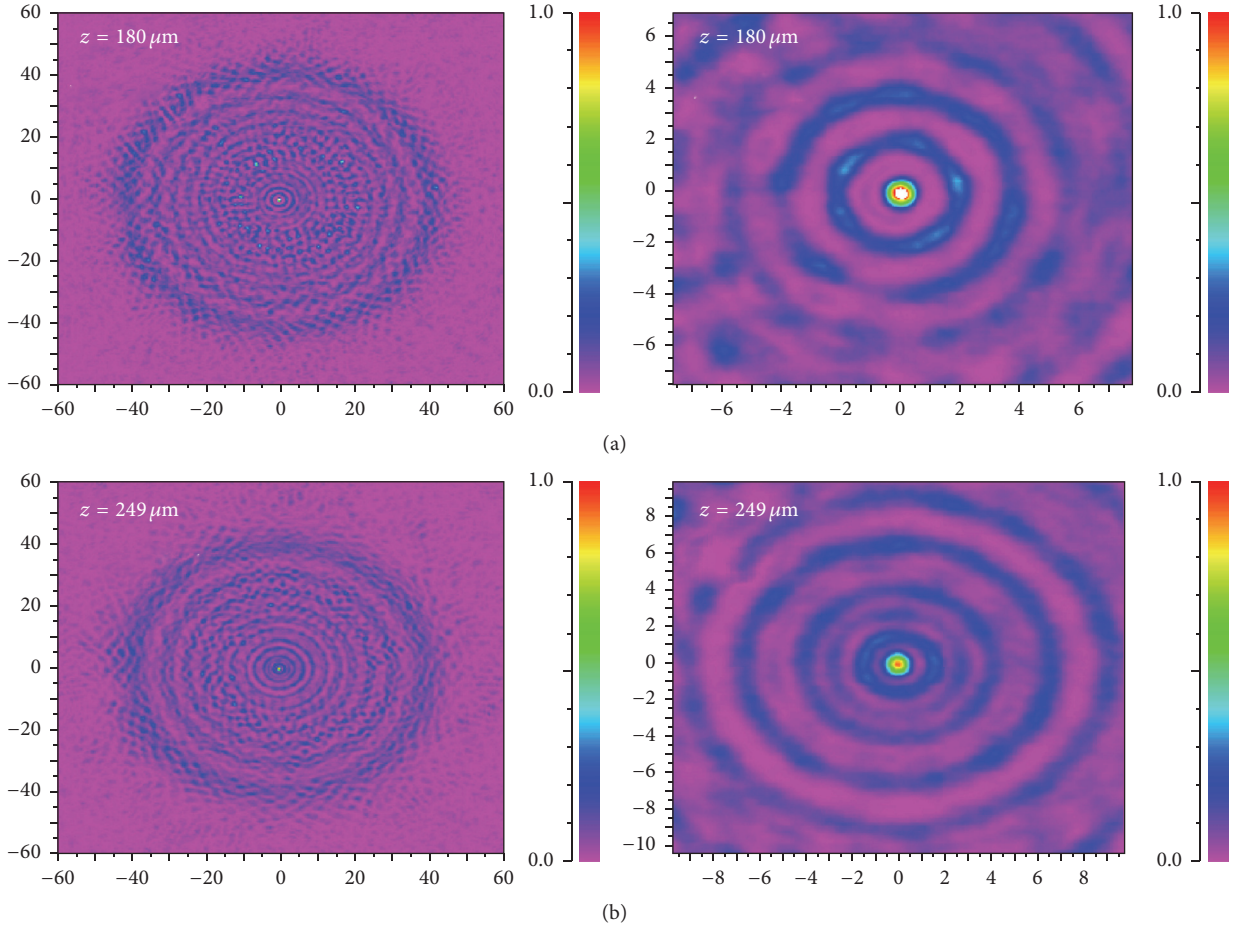

Figure 7: Transmitted, normalized intensity distribution in the XY plane (where the valve lies) calculated at 180 (a) and 249 (b) μm from the valve and for red light ($\lambda = 633$ nm); on right column, details of the same distributions are reported, for the sake of clarity.

Irradiating and imaging a single valve at different positions along the optical axis is not the only way to observe its ability to collect and concentrate light in local hotspots. In particular, Digital Holography (DH) allows the reconstruction of the optical field interacting with a single valve after the acquisition of its hologram. In [36, 38], diatom valve holograms have been acquired by means of a classical Mach-Zehnder interferometer. A polarized laser source emitting at a wavelength of $\lambda = 633$ nm was split in two beams, the reference and the object beam, respectively, by a polarized beam splitter. Microscope objectives were used along the path of the object beam, both to focus light onto a single valve deposited on a glass slide and to collect the light transmitted by the valve itself. A CCD plane array recorded the interference pattern, formed after both the object and the reference beams passed through a second, recombining beam splitter. After acquiring the interference pattern, the complex transmitted field (i.e., intensity plus phase) can be retrieved making use of the operator algebra proposed by Nazarathy and Shamir in [39], by which the Fresnel-Kirchhoff diffraction integral and the lens transfer factor are substituted by algebraic operators, bypassing the cumbersome integral calculus. Examples of intensity maps reconstructed at different positions along the optical axis after hologram acquisition (always for an incident wavelength $\lambda = 633$ nm) are reported in Figure 6(b) for *Actinoptychus senarius* and in Figure 8 for *C. wailesii*, respectively. Among the advantages of the operator algebra applied to DH, there is the possibility to retrieve light propagation in a medium different than air, just substituting the proper refractive index in the reconstruction algorithm. In Figure 8, for example, the field intensity has been reconstructed for a refractive index $n = 1.35$, corresponding to cytoplasm. Both DH [38] and previous WA-BPM numerical simulations [32] demonstrated that, in water and in cytoplasm, the confinement of incoming light takes place closer to the valve if compared to air, thus increasing light collection inside the cell.

At this point we can try to make some reasonable hypothesis on the correlation between photonic properties of diatom frustules and spatial distribution of chloroplasts inside the living cell. In particular, it is interesting to consider how chloroplasts relocate inside the cell according to illumination conditions. We already reminded (see Section 3 and [9]) that, for centric diatoms and in weak illumination conditions, it has been observed how chloroplasts tend to migrate close to the frustule walls thus coupling efficiently to the modes guided by girdles and valves. On the other hand, under

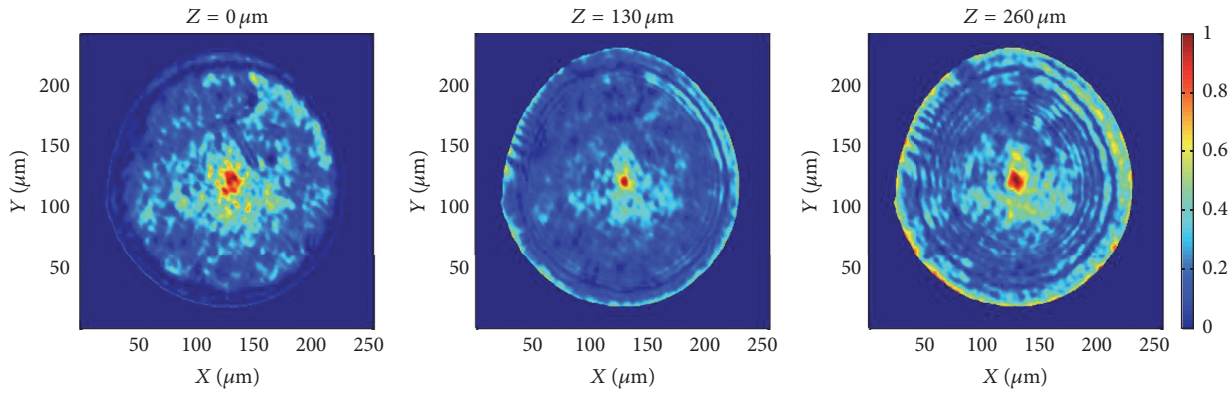

FIGURE 8: Reconstruction of light intensity transmitted by a diatom valve in cytoplasm: intensity maps at 0, 130, and 260 μm from the valve, respectively.

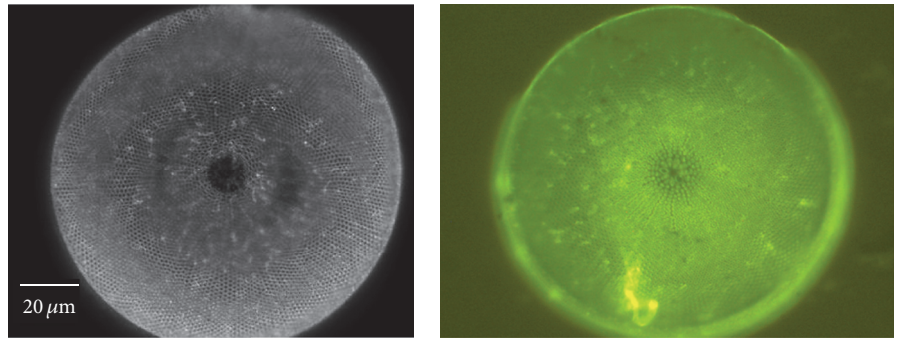

(a) (b)

FIGURE 9: Dark field image of a single valve of a *C. wailesii* diatom (a) and corresponding fluorescence macroscope image after excitation in the 450–490 nm spectral range (b).

intense irradiation, chloroplasts migrate towards the nucleus [28], that is, to the center of the cell, where visible light is mainly collected by means of the diffractive mechanism described above. This migration is enhanced for red light, as observed in [40], thus in the spectral interval where bot Noyes et al. [30] and Romann et al. [34] observed higher transmission of light through valves with respect to other wavelengths and where some of the absorption maxima of chlorophylls are located. Nevertheless, if we look at the penetration depth of sunlight through ocean [41], we can see how red radiation can penetrate at most to approximately 10–20 m, while light in the blue-violet range can penetrate up to almost 150 m. If we consider that, in this wavelength range, other more intense absorption maxima of chlorophylls are present, concurrent mechanisms of efficient light harvesting have to take place, as we will see in the next section.

5. Photoluminescence of Diatom Biosilica

It is known that the wide bandgap which characterizes bulk, amorphous silica does not allow any photoluminescence emission. Nevertheless, the various surface defects by which nanostructured silica is affected (mainly Si-OH and Si-H groups; nonbridging oxygen hole centers; self-trapped excitons) guarantee the presence of photoluminescence emission after excitation at the proper wavelengths [42].

Living diatoms present two main source of luminescence: frustule photoluminescence [43, 44] and autofluorescence from chloroplasts [38, 45] and lipid layers [46].

Besides the mentioned mechanisms at the origin of nanostructured silica photoluminescence, in the case of diatom frustules we have to mention also the contribution of organic residuals incorporated in the porous silica matrix [10, 47] and which are very difficult to remove even after severe treatment of the living cell with strong acid solutions.

In Figure 9 the image of a single valve of *C. wailesii* emitting green radiation after blue excitation in a wide spectral range (450–490 nm) is reported, while in Figure 10 photoluminescence spectra after excitation at 325 and 442 nm (emission wavelengths of a He-Cd laser) are shown.

It is interesting to notice how the photoluminescence process allows the conversion of UV radiation (harmful for DNA mainly through the formation of dimeric photoproducts between adjacent pyrimidines [48]) in blue radiation, where action spectrum of photosynthesis has one of its maxima (the other being placed, as we saw before, in red spectral

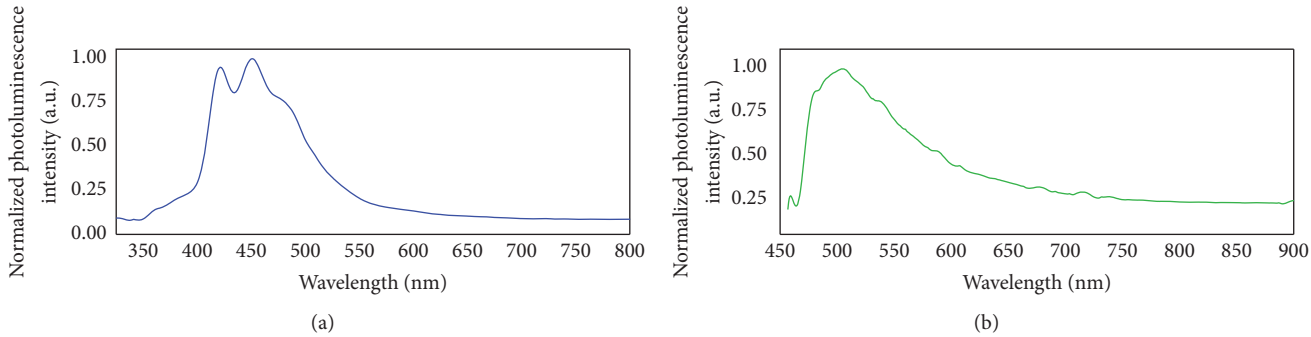

Figure 10: Photoluminescence spectra of *C. wailesii* diatom valves after excitations at 325 (a) and 442 nm (b), respectively.

region) [31]. Thus we can identify three specific mechanisms by which the frustule protects the living cell from detrimental UV radiation: absorption by amorphous porous silica; light-collection inhibition by diffraction; wavelength conversion by means of photoluminescent emission. However, systematic studies are still needed in order to better understand the complex relationship between the different optical properties of diatoms and their interaction with UV radiation [49].

6. Applications

First applications of diatom frustules date back to the Nineteenth century [6], when they were used as standards to test the resolving power of light microscope objectives [50]. Nowadays, the fossilized remain of diatom frustules, the so-called *diatomite* or *diatomaceous earth*, is routinely used in toothpaste and in some facial scrubs due to its abrasive property and in infiltration of water due to the submicron porosity of the material. Application of living diatoms include environmental monitoring and assessment of seas and freshwaters [51] and forensic science (starting from the analysis of the diatom content of dead bodies recovered from water) [52].

In the following we will mainly focus on applications strictly related to the optical properties described in previous Sections.

6.1. Metallized Frustules as Substrates for Surface Enhanced Raman Spectroscopy. It is well known that the irradiation of metallic-dielectric interfaces at the proper optical wavelength can excite surface plasmon polaritons (SPPs), that is, propagating fields due to collective oscillations of conductive electrons. In case of metallic nanostructures the excited field is well localized around the single metallic nanofeatures and we talk of localized surface plasmons (LSPs). LSPs are able to strongly enhance the Raman emission of molecules which stand in proximity of the metallic nanostructures, making possible what is called Surface Enhanced Raman Spectroscopy (SERS). Due to very high amplification factors, SERS compensates the low cross section of Raman scattering allowing the detection of single molecules.

In order to guarantee high levels of reproducibility, SERS substrates have to be characterized by extreme order and precision in the distribution of the nanofeatures, which is possible only recurring to very expensive top-down nanofabrication techniques. On the other side, the high reproduction rate of diatoms guarantee the availability of a massive number of very complex micro- and nanostructured dielectric structures which, properly metallized, could act as SERS substrates. In particular, we can reasonably hypothesize that the modes propagating in the valves and girdles of the frustules (see Section 3) can efficiently couple to the LSPs which can be sustained by the same valves and girdles after proper metallization [53].

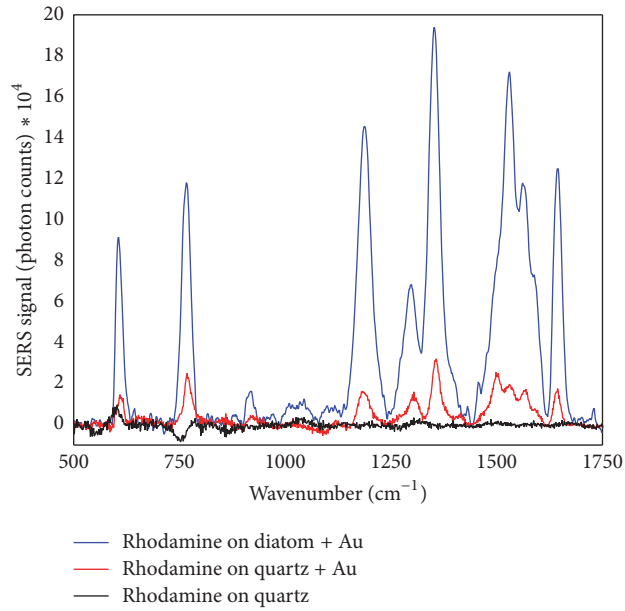

Figure 11: Raman spectra of rhodamine on quartz (black curve), rhodamine on quartz plus 20 nm of gold (red curve), and rhodamine on a single *C. wailesii* valve after 20 nm gold deposition (blue curve).

In Figure 11 some Raman spectra of rhodamine 6G deposited on different substrates are shown. In particular, the spectrum of rhodamine (10^{-5} M in water solution) deposited on a quartz slide is compared to the ones acquired on the same slide and on a diatom valve after deposition of 20 nm of gold. Gold has been deposited by means of thermal evaporation. Analyzing data an enhancement factor of about 9×10^2 can be retrieved comparing SERS and Raman intensities.

Besides thermal metal evaporation, other techniques can be exploited in order to obtain efficient SERS substrates starting from diatom frustules. Among others, Ren et al. [53]

incorporated silver nanoparticles in frustule of *Pinnularia* sp. diatom. More precisely, the nanoparticles were self-assembled onto an amine-functionalized, diatom-coated glass slide. This technique allowed obtaining an enhancement factor up to 12, comparing nonresonant Raman spectra of rhodamine 6G dropped on frustules and glass slide, respectively, both covered with silver nanoparticles.

In [54], a fabrication method that employs diatom frustules as templates for the formation of intricate microscaled and nanopatterned metallic structures is described. It is based on chemical removal of silica after frustule covering with a metal. The resulting metallic structures, if used as SERS substrates, guaranteed enhancement factors up to 10^6 (in case of silver and using a *Synedra* sp. frustule as template) for rhodamine as analyte and assuming a 100% coverage of the dye on the silver shell.

Kwon et al. [55] presented a method aimed at the covering of a substrate with a uniform diatom layer through a simple, low cost floating interface assembly technique. After assembling, *Coscinodiscus* sp. diatom layers have been functionalized by thin gold film deposition or by gold nanoparticle attachment. They observed, for methylene blue test molecules, enhancement factors of about 2×10^4 for gold film deposition and 7×10^4 for gold nanoparticles (due to stronger localization of the LSPs).

Other phenomena mediated by plasmonic effects have been observed starting from diatom frustules. Among all, very remarkable are the effects of extraordinary transmission observed in the infrared region of the spectrum through a gold replica of a single valve of *Coscinodiscus asteromphalus* diatom, obtained after metal coating and subsequent selective dissolution of silica [56]. Both experimental data and calculations suggest that the exhibited enhanced infrared transmission takes place through generation and mediation of surface plasmons.

6.2. Subdiffraction Light Squeezing. In the last few years several techniques have been proposed and tested in order to confine visible light below the diffraction limit in the far field, for example, making use of properly designed nanofabricated structures able to shape light beams and exploit the phenomenon of superoscillation [57, 58].

On other side, Optical Eigenmodes (OEi) technique [59] allows describing an optical system and its response to incident fields as a mode coupling problem and to determine the optimal excitation for a given, desired output: a superposition of initial fields is optimized such that the minimum/maximum measure is achieved. For example, the transmission through a pinhole is optimized by maximizing the energy flux through the pinhole itself or the spot focused by a microscope objective can be squeezed by minimizing the so-called *spot size operator* (SSO) defined, in scalar form, as

$$M_{jk}^{(2)} = \int_S \mathbf{r}^2 E_j^* E_k \, d\sigma, \tag{2}$$

where the probe fields $E_1 \cdots E_N$ are used as initial Hilbert basis with respect to which we define the OEi (experimentally, these probes are obtained by means of a spatial light modulator); the integral is evaluated over the region of interest S; $\mathbf{r}$ stands for the position vector.

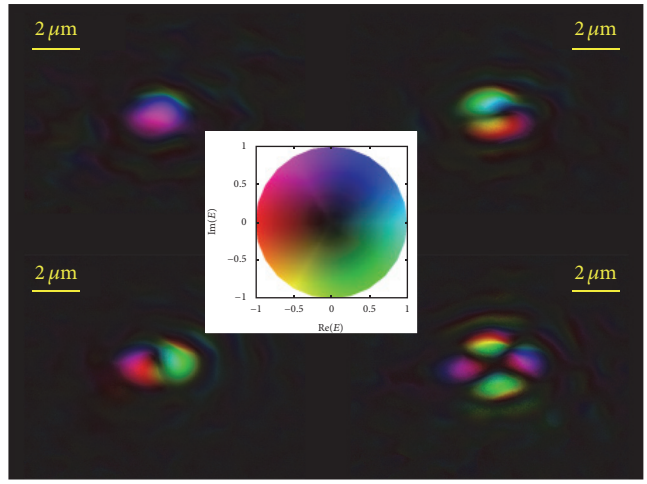

Figure 12: First four experimental eigenmodes contributing to the smallest squeezed spot through a single valve of *Arachnoidiscus* sp. diatom, with color encoding phase and brilliance encoding complex amplitude (see central legend).

OEi method has been recently combined with focusing properties of a single valve of *Arachnoidiscus* sp. [60] leading to light squeezing under the diffraction limit to an unprecedented level if compared to other far-field subdiffraction techniques reported in literature until then: working at 532 nm with circular polarization, a full width at half maximum of the transmitted spot of 0.21 λ/NA (with λ incident wavelength and NA numerical aperture of the system) is obtained, corresponding to a squeezing ratio of 41% with respect to the classical resolution limit of 0.51 λ/NA.

In Figure 12 the first four OEi contributing to minimization of the transmitted spot are represented in terms of phase (color) and amplitude (brilliance), while in Figure 13 the light spot transmitted by a single valve and detected at a distance of 20 μm from it is visualized under different conditions. In (a) the spot is affected only by the focusing property of the valve. In (b) the point spread function (PSF) through the quartz slide on which the valve was placed is shown. PSF is, in this case, defined as the combination of OEi that decompose a Dirac function and it corresponds to the local aberration correction of the optical system. In (c) the PSF relative to the valve is reported while finally, in (d), the squeezed spot transmitted by the valve after the minimization of the SSO is reported. The presence, in the squeezed spot, of sidebands which always accompany all linear subdiffraction focusing methods has to be noticed.

6.3. Light Trapping for Solar Applications. The ability of diatom frustules to collect and confine light with high efficiency can be exploited in the development of new biobased or bioinspired solar cells if properly chemically modified [61].

In [62], for example, diatom frustules were coated with titania nanoparticles (less than 20 nm in diameter) by means of plasma treatment (thus avoiding any linking agent) and

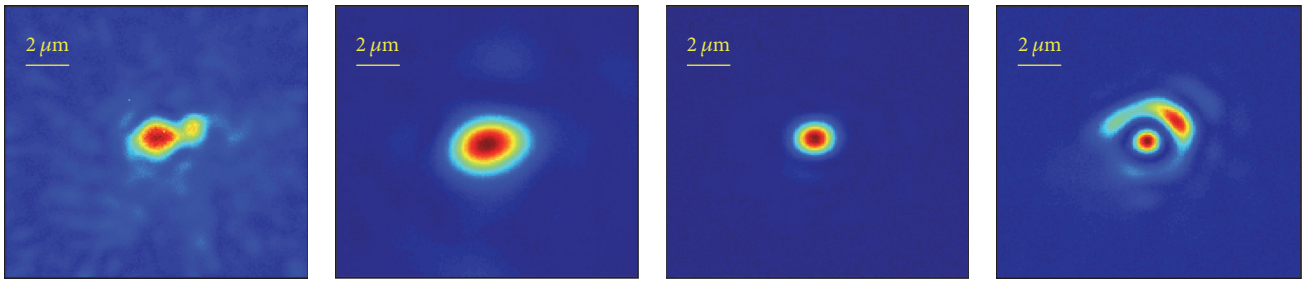

FIGURE 13: Transmitted intensity distributions in the xy plane at a distance $z = 20\,\mu$m from the diatom valve. Spot focused by valve alone (a); PSF of the glass slide (b); PSF of the valve (c); OEi squeezed spot (d).

used in dye sensitized solar cells (DSSCs) in order to improve their efficiency. In this kind of cells the dye generates, after absorption of light, electrons that are excited into the conduction band of a semiconductor (usually thin films of titania, indeed) which then travel to the working electrode. Titania-functionalized frustules allow to obtain three-dimensional titania structures with high specific surface, thus increasing the interaction between titania nanoparticles themselves and dye electrons. After only three cycles of plasma treatment, an increase of DSSC efficiency of about 30% with respect to the use of titania thin films has been achieved.

Besides the application of modified frustules in improving solar cells efficiency, a biomimetic approach can also be applied. Wang et al. [63], for example, applied genetic algorithms to the design of light-trapping structures, mimicking the evolution of periodic, natural photonic structures, reaching estimated enhancement factors over three times the Yablonovitch limit.

6.4. Diatom-Based Sensors and Biosensors. Diatom photoluminescence characteristics, in terms of both involved intensities and spectral features, are strongly dependent by the chemical composition of the surrounding environment. This property, together with the high specific surface of porous biosilica, makes diatom frustules very suitable in optical sensing.

It has been observed [64] that, in presence of electrophilic gases or vapors such as NO_2, acetone, and ethanol, the photoluminescence spectra of *Thalassiosira rotula* frustules (peaked around 533 nm in air after excitation at 325 nm) are progressively quenched and red-shifted. On the other side, the exposure to nucleophilic gases like xylene and pyridine causes, apart from the above-mentioned red shift in the emission spectra, a noticeable enhancement of the photoluminescence intensity. An extension of this study to other species (*C. wailesii* and *Cocconeis scutellum* [65, 66]) allowed observing different responses of photoluminescence to gases concentration and different ranges of sensitivity varying the species and, thus, the morphology of the frustules and the dimensions and arrangements of their pores.

Even though gas sensors based on frustule photoluminescence are characterized by high specificity (i.e., different gases produce different and distinct spectral responses), they lack selectivity, (i.e., they are not able to distinguish among different analytes in a mixture). This can be fixed by linking to the frustule surface molecules which, acting like probes, are able to selectively bond to specific analytes. Typically, biomacromolecules such as proteins (enzymes, antibodies, etc.) and single strands of DNA or RNA are used as bioprobes. A possible way to link such molecules to diatom silica is to use an organosilane compound such as the aminopropyltriethoxysilane (APTES) and a functional cross-linker such as glutaraldehyde (GA), which reacts with the amino groups on the silanized surface and coats the surface of the frustule with another thin layer of molecules [67]. Such a modified surface works as an active substrate which allows the attachment of the biological probes [68].

In Figure 14 a comparison of photoluminescence spectrum of bare *Cyclotella* sp. biosilica with those obtained after functionalization with rabbit-IgG antibody and rabbit-IgG antibody-antigen complex is shown (from [69]).

7. Conclusions

In this paper all the main optical properties of diatom frustules have been reviewed, trying to link them, when possible, to functions and properties of the living cell. In addition to representing an evolutionary advantage in efficient collection and exploitation of sunlight in aqueous environment where it is not easily accessible, these properties can also find application in several technological fields.

Other possible applications of frustules, not only or not strictly related to their photonic properties, need to be mentioned: porous nanoparticles obtained from diatomite can be used, if properly chemically functionalized, in a drug delivery system, for example, for cancer therapy [70, 71]; nanoscale germanium and titanium particles have been incorporated in diatom frustules by means of bioreactor processes in silicon starvation, for possible applications in optoelectronics [23, 24]; diatom silica frustules can be used as templates to fabricate replicas of different materials, such as gold [25] or polymers [27] or they can be reduced into silicon [26] for possible applications as optical elements, masters for nanofabrications, biosensing device components, and nanoreactors; diatomite and biofilm frustules have been used as scatterers in PMMA matrix composite random lasers containing rhodamine B as gain medium [72]; finally, the proper engineering of the genes involved in silaffins encoding

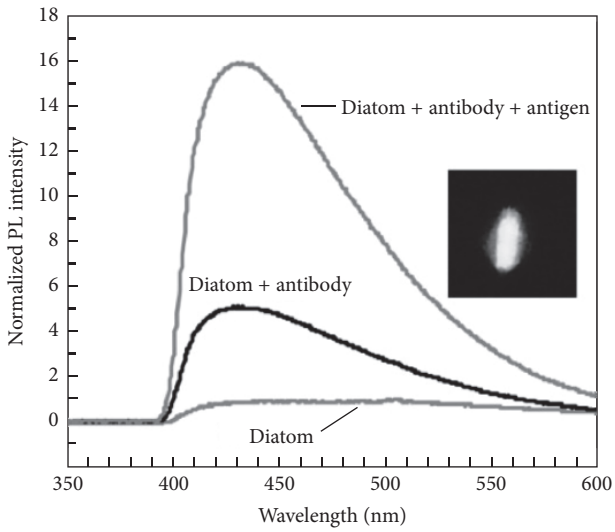

Figure 14: Variation of intensity in photoluminescence spectra of *Cyclotella* sp. frustule after functionalization with rabbit-IgG antibody and linking with its antigen. Inset: photoluminescence emission from antibody-functionalized diatom biosilica. Reproduced with permission from [69].

could lead to the design and fabrication of frustules with the desired shape and morphology [16].

Competing Interests

The author declares that there is no conflict of interests regarding the publication of this paper.

Acknowledgments

The author thanks Mario De Stefano from the Department of Environmental, Biological and Pharmaceutical Sciences and Technologies of the Second University of Naples and Luca De Stefano from the Institute for Microelectronics and Microsystems of the Italian National Research Council for introducing him to the fascinating world of diatoms and their photonic properties; Anna Chiara De Luca and Stefano Managò from the Institute of Protein Biochemistry of the Italian National Research Council for Raman and SERS characterization of the frustules; Giuseppe Di Caprio from Harvard Medical School, Cambridge, MA, USA, for having introduced the application of digital holography to the study of optical properties of diatoms; Ilaria Rea from the Institute for Microelectronics and Microsystems of the Italian National Research Council for photoluminescence spectroscopy measurements; Michael Mazilu from School of Physics & Astronomy, University of St. Andrews, Scotland, UK, for his intuition about the application of OEi technique to the squeezing of light through diatom valves.

References

[1] P. Vukusic and J. R. Sambles, "Photonic structures in biology," *Nature*, vol. 424, no. 6950, pp. 852–855, 2003.

[2] A. R. Parker and H. E. Townley, "Biomimetics of photonic nanostructures," *Nature Nanotechnology*, vol. 2, no. 6, pp. 347–353, 2007.

[3] M. Kolle, *Photonic Structures Inspired by Nature*, Springer, 2011.

[4] V. Greanya, *Bioinspired Photonics: Optical Structures and Systems Inspired by Nature*, CRC Press, Taylor and Francis Group, New York, NY, USA, 2016.

[5] D. M. Nelson, P. Tréguer, M. A. Brzezinski, A. Leynaert, and B. Quéguiner, "Production and dissolution of biogenic silica in the ocean: revised global estimates, comparison with regional data and relationship to biogenic sedimentation," *Global Biogeochemical Cycles*, vol. 9, no. 3, pp. 359–372, 1995.

[6] F. E. Round, R. M. Crawford, and D. G. Mann, *The Diatoms*, Cambridge University Press, Cambridge, UK, 1990.

[7] D. Losic, R. J. Pillar, T. Dilger, J. G. Mitchell, and N. H. Voelcker, "Atomic Force Microscopy (AFM) characterisation of the porous silica nanostructure of two centric diatoms," *Journal of Porous Materials*, vol. 14, no. 1, pp. 61–69, 2007.

[8] H. E. Townley, "Diatom frustules: physical, optical, and biotechnological applications," in *The Diatom World*, Springer, 2011.

[9] T. Fuhrmann, S. Landwehr, M. El Rharbi-Kucki, and M. Sumper, "Diatoms as living photonic crystals," *Applied Physics B: Lasers and Optics*, vol. 78, no. 3, pp. 257–260, 2004.

[10] M. Kammer, R. Hedrich, H. Ehrlich, J. Popp, E. Brunner, and C. Krafft, "Spatially resolved determination of the structure and composition of diatom cell walls by Raman and FTIR imaging," *Analytical and Bioanalytical Chemistry*, vol. 398, no. 1, pp. 509–517, 2010.

[11] R. Simó, "Production of atmospheric sulfur by oceanic plankton: biogeochemical, ecological and evolutionary links," *Trends in Ecology and Evolution*, vol. 16, no. 6, pp. 287–294, 2001.

[12] A. J. Watson and P. S. Liss, "Marine biological controls on climate via the carbon and sulphur geochemical cycles," *Philosophical Transactions of the Royal Society B: Biological Sciences*, vol. 353, no. 1365, pp. 41–51, 1998.

[13] J. C. Lewin, "Silicon metabolism in diatoms. Evidence of the role of reduced sulfur compounds in silicon utilization," *Journal of General Physiology*, vol. 54, pp. 589–599, 1954.

[14] M. Hildebrand, K. Dahlin, and B. E. Volcani, "Characterization of a silicon transporter gene family in Cylindrotheca fusiformis: sequences, expression analysis, and identification of homologs in other diatoms," *Molecular and General Genetics*, vol. 260, no. 5, pp. 480–486, 1998.

[15] N. Kröger, R. Deutzmann, and M. Sumper, "Polycationic peptides from diatom biosilica that direct silica nanosphere formation," *Science*, vol. 286, no. 5442, pp. 1129–1132, 1999.

[16] N. Kröger and N. Poulsen, "Diatoms—from cell wall biogenesis to nanotechnology," *Annual Review of Genetics*, vol. 42, pp. 83–107, 2008.

[17] J. D. Joannopoulos, S. G. Johnson, J. N. Winn, and R. D. Meade, *Photonic Crystals: Molding the Flow of Light*, Princeton University Press, 2nd edition, 2008.

[18] R. T. Lee and G. S. Smith, "Detailed electromagnetic simulation for the structural color of butterfly wings," *Applied Optics*, vol. 48, no. 21, pp. 4177–4190, 2009.

[19] T. A. Birks, P. J. Roberts, P. S. J. Russell, D. M. Atkin, and T. J. Shepherd, "Full 2-D photonic bandgaps in silica/air structures," *Electronics Letters*, vol. 31, no. 22, pp. 1941–1943, 1995.

[20] L. De Stefano, P. Maddalena, L. Moretti et al., "Nano-biosilica from marine diatoms: a brand new material for photonic applications," *Superlattices and Microstructures*, vol. 46, no. 1-2, pp. 84–89, 2009.

[21] K. Kieu, C. Li, Y. Fang et al., "Structure-based optical filtering by the silica microshell of the centric marine diatom *Coscinodiscus wailesii*," *Optics Express*, vol. 22, no. 13, pp. 15992–15999, 2014.

[22] R. D. Meade, A. M. Rappe, K. D. Brommer, J. D. Joannopoulos, and O. L. Alerhand, "Accurate theoretical analysis of photonic band-gap materials," *Physical Review B*, vol. 48, no. 11, pp. 8434–8437, 1993.

[23] C. Jeffryes, T. Gutu, J. Jiao, and G. L. Rorrer, "Metabolic insertion of nanostructured TiO_2 into the patterned biosilica of the diatom *Pinnularia* sp. by a two-stage bioreactor cultivation process," *ACS Nano*, vol. 2, no. 10, pp. 2103–2112, 2008.

[24] C. Jeffryes, T. Gutu, J. Jiao, and G. L. Rorrer, "Two-stage photobioreactor process for the metabolic insertion of nanostructured germanium into the silica microstructure of the diatom *Pinnularia* sp.," *Materials Science and Engineering C*, vol. 28, no. 1, pp. 107–118, 2008.

[25] D. Losic, J. G. Mitchell, and N. H. Voelcker, "Fabrication of gold nanostructures by templating from porous diatom frustules," *New Journal of Chemistry*, vol. 30, no. 6, pp. 908–914, 2006.

[26] Z. Bao, M. R. Weatherspoon, S. Shian et al., "Chemical reduction of three-dimensional silica micro-assemblies into microporous silicon replicas," *Nature*, vol. 446, no. 7132, pp. 172–175, 2007.

[27] D. Losic, J. G. Mitchell, R. Lal, and N. H. Voelcker, "Rapid fabrication of micro- and nanoscale patterns by replica molding from diatom biosilica," *Advanced Functional Materials*, vol. 17, no. 14, pp. 2439–2446, 2007.

[28] T. Furukawa, M. Watanabe, and I. Shihira-Ishikawa, "Green- and blue-light-mediated chloroplast migration in the centric diatom *Pleurosira laevis*," *Protoplasma*, vol. 203, no. 3, pp. 214–220, 1998.

[29] L. De Stefano, I. Rea, I. Rendina, M. De Stefano, and L. Moretti, "Lensless light focusing with the centric marine diatom *Coscinodiscus walesii*," *Optics Express*, vol. 15, no. 26, pp. 18082–18088, 2007.

[30] J. Noyes, M. Sumper, and P. Vukusic, "Light manipulation in a marine diatom," *Journal of Materials Research*, vol. 23, no. 12, pp. 3229–3235, 2008.

[31] J. T. O. Kirk, *Light and Photosynthesis in Aquatic Ecoystems*, Cambridge University Press, 2011.

[32] E. De Tommasi, I. Rea, V. Mocella et al., "Multi-wavelength study of light transmitted through a single marine centric diatom," *Optics Express*, vol. 18, no. 12, pp. 12203–12212, 2010.

[33] S.-H. Hsu, C. Paoletti, M. Torres, R. J. Ritchie, A. W. D. Larkum, and C. Grillet, "Light transmission of the marine diatom Coscinodiscus wailesii," in *Proceedings of the SPIE 8339, Bioinspiration, Biomimetics, and Bioreplication*, vol. 8339, April 2012.

[34] J. Romann, J.-C. Valmalette, M. S. Chauton, G. Tranell, M.-A. Einarsrud, and O. Vadstein, "Wavelength and orientation dependent capture of light by diatom frustule nanostructures," *Scientific Reports*, vol. 5, Article ID 17403, 2015.

[35] J. Romann, J.-C. Valmalette, A. Røyset, and M.-A. Einarsrud, "Optical properties of single diatom frustules revealed by confocal microspectroscopy," *Optics Letters*, vol. 40, no. 5, pp. 740–743, 2015.

[36] M. A. Ferrara, P. Dardano, L. De Stefano et al., "Optical properties of diatom nanostructured biosilica in *Arachnoidiscus* sp: micro-optics from mother nature," *PLoS ONE*, vol. 9, no. 7, Article ID e103750, 2014.

[37] N. E. Brown, *Arachnoidiscus. An Account of the Genus, Comprising its History, Distribution, Development and Growth of the Frustule, Structure and its Examination and Purpose in Life, and a Key to and Descriptions of all Known Species, Illustrated*, W. Watson & Sons, London, UK, 1933.

[38] G. Di Caprio, G. Coppola, L. D. Stefano et al., "Shedding light on diatom photonics by means of digital holography," *Journal of Biophotonics*, vol. 7, no. 5, pp. 341–350, 2014.

[39] M. Nazarathy and J. Shamir, "Fourier optics described by operator algebra," *Journal of the Optical Society of America*, vol. 70, no. 2, pp. 150–159, 1980.

[40] I. Shihira-Ishikawa, T. Nakamura, S.-I. Higashi, and M. Watanabe, "Distinct responses of chloroplasts to blue and green laser microbeam irradiations in the centric diatom *Pleurosira laevis*," *Photochemistry and Photobiology*, vol. 83, no. 5, pp. 1101–1109, 2007.

[41] C. M. Lalli and T. R. Parsons, *Biological Oceanography. An Introduction*, Elsevier, Amsterdam, The Netherlands, 2nd edition, 1997.

[42] T. Qin, T. Gutu, J. Jiao, C.-H. Chang, and G. L. Rorrer, "Photoluminescence of silica nanostructures from bioreactor culture of marine diatom Nitzschia frustulum," *Journal of Nanoscience and Nanotechnology*, vol. 8, no. 5, pp. 2392–2398, 2008.

[43] E. De Tommasi, I. Rendina, I. Rea, M. De Stefano, A. Lamberti, and L. De Stefano, "Intrinsic photoluminescence of diatom shells in sensing applications," in *Optical Sensors*, vol. 7356 of *Proceedings of SPIE*, 15 pages, 2009.

[44] N. Mazumder, A. Gogoi, R. D. Kalita, G. A. Ahmed, A. K. Buragohain, and A. Choudhury, "Luminescence studies of fresh water diatom frustules," *Indian Journal of Physics*, vol. 84, no. 6, pp. 665–669, 2010.

[45] P. LeDuff, G. Roesijadi, and G. L. Rorrer, "Micro-photoluminescence of single living diatom cells," *Luminescence*, vol. 31, no. 7, pp. 1379–1383, 2016.

[46] K. Kieu, S. Mehravar, R. Gowda, R. A. Norwood, and N. Peyghambarian, "Label-free multi-photon imaging using a compact femtosecond fiber laser mode-locked by carbon nanotube saturable absorber," *Biomedical Optics Express*, vol. 4, no. 10, pp. 2187–2195, 2013.

[47] M. Kucki, *Biological photonic crystals: diatoms. dye functionalization of biological silica nanostructures [Ph.D. thesis]*, University of Kassel, Kassel, Germany, 2009.

[48] J. Kiefer, *Biological Radiation Effects*, Springer, Berlin, Germany, 1990.

[49] M. Ellegaard, T. Lenau, N. Lundholm et al., "The fascinating diatom frustule—can it play a role for attenuation of UV radiation?" *Journal of Applied Phycology*, 2016.

[50] G. R. Hasle and G. A. Fryxell, "Diatoms: cleaning and mounting for light and electron microscopy," *Transactions of the American Microscopical Society*, vol. 89, no. 4, pp. 469–474, 1970.

[51] E. F. Stoermer and J. P. Smol, *The Diatoms. Applications for the Environmental and Earth Science*, Cambridge University Press, 2004.

[52] K. Verma, "Role of diatoms in the world of forensic science," *Journal of Forensic Research*, vol. 4, no. 2, Article ID 1000181, 2013.

[53] F. Ren, J. Campbell, G. L. Rorrer, and A. X. Wang, "Surface-enhanced raman spectroscopy sensors from nanobiosilica with self-assembled plasmonic nanoparticles," *IEEE Journal on Selected Topics in Quantum Electronics*, vol. 20, no. 3, Article ID 6900806, 2014.

[54] E. K. Payne, N. L. Rosi, C. Xue, and C. A. Mirkin, "Sacrificial biological templates for the formation of nanostructured metallic

microshells," *Angewandte Chemie—International Edition*, vol. 44, no. 32, pp. 5064–5067, 2005.

[55] S. Y. Kwon, S. Park, and W. T. Nichols, "Self-assembled diatom substrates with plasmonic functionality," *Journal of the Korean Physical Society*, vol. 64, no. 8, pp. 1179–1184, 2014.

[56] Y. Fang, V. W. Chen, Y. Cai et al., "Biologically enabled syntheses of freestanding metallic structures possessing subwavelength pore arrays for extraordinary (surface plasmon-mediated) infrared transmission," *Advanced Functional Materials*, vol. 22, no. 12, pp. 2550–2559, 2012.

[57] E. T. F. Rogers, J. Lindberg, T. Roy et al., "A super-oscillatory lens optical microscope for subwavelength imaging," *Nature Materials*, vol. 11, no. 5, pp. 432–435, 2012.

[58] E. T. F. Rogers, S. Savo, J. Lindberg, T. Roy, M. R. Dennis, and N. I. Zheludev, "Super-oscillatory optical needle," *Applied Physics Letters*, vol. 102, no. 3, Article ID 031108, 2013.

[59] M. Mazilu, J. Baumgartl, S. Kosmeier, and K. Dholakia, "Optical eigenmodes; exploiting the quadratic nature of the energy flux and of scattering interactions," *Optics Express*, vol. 19, no. 2, pp. 933–945, 2011.

[60] E. De Tommasi, A. C. De Luca, L. Lavanga et al., "Biologically enabled sub-diffractive focusing," *Optics Express*, vol. 22, no. 22, pp. 27214–27227, 2014.

[61] C. Jeffryes, J. Campbell, H. Li, J. Jiao, and G. Rorrer, "The potential of diatom nanobiotechnology for applications in solar cells, batteries, and electroluminescent devices," *Energy & Environmental Science*, vol. 4, no. 10, pp. 3930–3941, 2011.

[62] J. Toster, K. S. Iyer, W. Xiang, F. Rosei, L. Spiccia, and C. L. Raston, "Diatom frustules as light traps enhance DSSC efficiency," *Nanoscale*, vol. 5, no. 3, pp. 873–876, 2013.

[63] C. Wang, S. Yu, W. Chen, and C. Sun, "Highly efficient light-trapping structure design inspired by natural evolution," *Scientific Reports*, vol. 3, article no. 1025, 2013.

[64] L. De Stefano, I. Rendina, M. De Stefano, A. Bismuto, and P. Maddalena, "Marine diatoms as optical chemical sensors," *Applied Physics Letters*, vol. 87, no. 23, Article ID 233902, pp. 1–3, 2005.

[65] A. Setaro, S. Lettieri, P. Maddalena, and L. De Stefano, "Highly sensitive optochemical gas detection by luminescent marine diatoms," *Applied Physics Letters*, vol. 91, no. 5, Article ID 051921, 2007.

[66] S. Lettieri, A. Setaro, L. De Stefano, M. De Stefano, and P. Maddalena, "The gas-detection properties of light-emitting diatoms," *Advanced Functional Materials*, vol. 18, no. 8, pp. 1257–1264, 2008.

[67] L. De Stefano, A. Lamberti, L. Rotiroti, and M. De Stefano, "Interfacing the nanostructured biosilica microshells of the marine diatom *Coscinodiscus wailesii* with biological matter," *Acta Biomaterialia*, vol. 4, no. 1, pp. 126–130, 2008.

[68] L. De Stefano, L. Rotiroti, M. De Stefano et al., "Marine diatoms as optical biosensors," *Biosensors and Bioelectronics*, vol. 24, no. 6, pp. 1580–1584, 2009.

[69] D. K. Gale, T. Cutu, J. Jiao, C.-H. Chang, and G. L. Rorrer, "Photoluminescence detection of biomolecules by antibody-functionalized diatom biosilica," *Advanced Functional Materials*, vol. 19, no. 6, pp. 926–933, 2009.

[70] M. Terracciano, M.-A. Shahbazi, A. Correia et al., "Surface bioengineering of diatomite based nanovectors for efficient intracellular uptake and drug delivery," *Nanoscale*, vol. 7, no. 47, pp. 20063–20074, 2015.

[71] B. Delalat, V. C. Sheppard, S. Rasi Ghaemi et al., "Targeted drug delivery using genetically engineered diatom biosilica," *Nature Communications*, vol. 6, article no. 8791, 2015.

[72] F. R. Lamastra, R. De Angelis, A. Antonucci et al., "Polymer composite random lasers based on diatom frustules as scatterers," *RSC Advances*, vol. 4, no. 106, pp. 61809–61816, 2014.